JOURNAL OF NANOFLUIDS

http://www.aspbs.com/jon/

Accepted September 17th, 2024.

Electro-Osmotic Peristaltic Streaming Flow of a Fractional Second-Grade Viscoelastic Fluid in a Tube with Permeable Walls Containing Single and Multi-Wall Carbon Nanotubes.

Mahadev M Channakote[1*], O. Anwar Bég[2], Mahesha Narayana[3], M. Shekar[4] and N.S. Akbar[5]

[1*]*Department of Mathematics and Statistics, M. S. Ramaiah University of Applied Science, Bengaluru, Karnataka, 560054, India.*

[2]*Professor and Director-Multi-Physical Engineering Sciences Group (MPESG), Mechanical Engineering Department, Corrosion/Coating Lab., 3-08, SEE Building, University of Salford, Manchester, M54WT, **UK**.*

[3]*Department of Mathematics, The University of the West Indies, Mona Campus, Kingston, **Jamaica**.*

[4]*Department of Mathematics, B. M. S. College of Engineering, Bengaluru, India.*

[5]*Department of Mechanical Engineering, College of Engineering, Prince Mohammad Bin Fahd University, Al Khobar 31952, Saudi Arabia*

**Corresponding author*- Email: mchannakote@rediffmail.com

ABSTRACT:

This paper develops a mathematical model to analyse the behaviour of a viscoelastic nanofluid flowing through a radially symmetric cylindrical duct with a permeable wall, incorporating electro-osmotic effects. The model employs a fractional viscoelastic Reiner-Rivlin differential equation using Caputo's definition to characterize the fluid's rheology, and includes considerations of heat generation and natural convection. Electro-osmotic dynamics are analysed using the Debye-Hückel approximation. The study investigates the impact of single-walled carbon nanotubes (SWCNTs) and multi-walled carbon nanotubes (MWCNTs) on flow characteristics, focusing on the thermal and electrical properties of blood. By applying suitable scaling transformations, the partial differential equations are reduced to an ordinary differential equation system. Analytical solutions are obtained for the non-dimensional boundary value problem, and key parameters such as axial velocity, temperature, electrical potential, volumetric flow rate, and pressure gradient are computed and visualized using Mathematica. The results are significant for modelling flow dynamics in the human oesophagus and have practical implications for nanoparticle-based applications in cancer diagnosis, angiography, and angioplasty. The study finds that carbon nanotube (CNTs) enhances thermal conductivity and fluid velocity, and that increased thermal source/sink parameters (β_1) raise temperature, while higher (CNT) carbon nanotubes volume fractions (ϕ) reduce temperature, with Multi walled carbon nanotube (MWCNTs) achieving higher temperatures.

KEYWORDS: *Carbon nanotubes, electro-osmosis, fractional second-grade fluid model, Caputo's definition, Debye-Huckel linearization, Peristalsis, Permeable wall.*

1. INTRODUCTION:

The study of peristaltic flow has extensive applications in biomedical engineering and industrial processes. It is a form of liquid movement that develops physiologically in the human body. Several of its characteristics are seen in biological formations. Peristalsis, characterized by the rhythmic contractions and relaxations of tube, channel, or duct walls, drives fluid movement and is commonly observed in processes such as blood flow in arteries and veins, saliva secretion, sperm transport, cerebrospinal fluid flow, and food passage through the digestive tract. This phenomenon is also central to the functioning of medical devices like insulin pumps, glucose sensors, bio-mimetic capillaries, blood pumps, oxygenators, dialysis machines, and ventilators. To better understand the peristaltic action of non-Newtonian bio-rheological fluids, researchers have conducted various theoretical and computational studies under different assumptions. Mathematical fluid mechanics investigations of

peristaltic pumping started considerably later, in the 1960s, and used the Navier-Stokes equations as model equations for a viscous fluid, even though peristaltic processes were recognized over a century before in physiology. In order to significantly simplify the mathematics of peristaltic transport, Yin and Fung[1] and Shapiro et al[2]. made significant contributions. They provided lubrication approximations and remapped the moving boundary value issue to a stationary (wave) frame of reference. Many researchers have since taken up this idea and used it in situations where the pumped fluid must either be non-corrosive to prevent it from coming into contact with the working parts of standard pumping systems or stay uncontaminated, as in the case of blood. Most recently, numerous concepts of physics such as heat transfer, porous media, entropy and exergy, radiation, chemical reaction, rheology, electro-osmosis, variable viscosity, etc., have been considered in peristaltic pumping models and have reported many significant results. An abundant exploration of the topic of various liquid flow with various geometries under external effect is well reported in the literature[3-11].

Nanofluids exhibit unique thermal, electrical, and rheological properties compared to traditional fluids, making them attractive for various industrial and scientific applications. The addition of nanoparticles to a base fluid can enhance heat transfer efficiency, improve lubrication properties, and increase the stability and performance of the fluid in different conditions. Researchers continue to explore the potential of nanofluids in diverse fields, including cooling systems for electronics, solar energy harvesting, drug delivery systems, and advanced manufacturing processes. The ability to tailor the properties of nanofluids by adjusting the type, size, and concentration of nanoparticles opens up new possibilities for innovation and optimization in numerous applications. The term "nanofluid" was first used in 1995 at Argonne National Laboratory by Choi[12]. In his research, he found that nanofluids required less pumping power compared to pure liquids to achieve the same level of heat transfer intensification and particle clogging, which helped reduce the size of the system. Buongiorno[13] developed a two-component nanoscale model that considers both mass diffusion (nanoparticle concentration) and heat diffusion, emphasizing the importance of both processes in the dynamics of nanofluids. In a recent work, Biswas et al.[14] explored a wavy-walled, tilted porous enclosure filled with hybrid nanofluid and imposing a partially active magnetic field in the narrative. The effect of wall curvature on heat transmission, entropy production, and magneto-nanofluidic flow in a semicircular thermal annular system was studied by Biwas et al[14]. The analysis considered fluid volume and cooling surface limitations as constant factors. Some more relevant article related to the topic are cited in Refs[15-19].

Peristaltic flows of nanofluids have been extensively researched computationally and theoretically due to their potential applications in biomedicine and energy devices. Nanofluids are colloidal suspensions of nanoparticles in a base fluid, and their unique thermal and rheological properties make them ideal for various applications. In peristaltic transport, which involves the movement of fluid through pulsating contractions and expansions, nanofluids offer several advantages. The addition of nanoparticles improves the fluid's thermal conductivity, viscosity, and heat transfer efficiency, making them beneficial for applications such as drug delivery systems where precise control over temperature and fluid properties is crucial. Recently, there has been some apparent addition to the study of peristalsis through the interaction of nanoparticles under various physiological situations. In the peristaltic literature nanofluid was first introduced by Nadeem and Akbar[20]. A homotropy perturbation strategy was used by Akbar et al.[21] to relate the temperature and nanoparticle equations while studying the peristaltic flow of nanofluids in a diverging tube. The findings showed that elevated thermophoresis numbers and Brownian motion parameters led to higher temperatures, but an increase in pressure rise had the opposite effect. The peristaltic flow of nanofluids and its use in drug delivery devices was covered by Tripathi et al[22]. Motivated by applications in pharmacodynamics, they investigated how temperature and species Grashoff numbers, thermophoretic body force parameters, Brownian motion, and velocity affected temperature gradient distributions, pressure gradient distributions, and the proportion of nanoparticles using Buongiorno's model. Nadeem et al.[23] focused on investigating the impact of heat

and mass transfer on the peristaltic flow of the nanofluid between eccentric cylinders. The references are a collection of some of the more creative and groundbreaking studies that have examined the peristaltic transport of nanofluids.[24-27]

In recent years, peristaltic streaming flows involving single-walled carbon nanotubes (SWCNTs) and multi-walled carbon nanotubes (MWCNTs) have gained prominence. This innovative approach utilizes carbon nanotubes to enhance the thermal properties of both industrial and physiological materials. Nanotubes, particularly CNTs, with their exceptional thermal characteristics, are incorporated into fundamental industrial materials to augment their thermal properties. Various nanoparticles, including aluminium, copper, zinc oxides, and carbon nanotubes, are extensively employed to improve the thermal capabilities of base liquids. CNTs, distinguished by their enhanced thermal conductivities, versatile mechanical structures, and remarkable electrical properties, are recognized as precise tools for achieving desired fluid features. Given these distinctive qualities, CNTs have become a focal point of intensive research across diverse domains. For instance, carbon nanotubes can serve as scaffolding material for tissue engineering. By mimicking the natural structure of muscle tissues, nanotubes can be incorporated into artificial muscle constructs to support tissue regeneration. This application may aid in repairing damaged or diseased parts of the gastrointestinal tract. Peristaltic transport in single-walled and multi-walled carbon nanotubes is modelled and interpreted using Newtonian heating and entropy optimization techniques. Some scholars have recently made intriguing contributions, which are emphasized in this article. A review of the progress made by carbon-based nanofluids in heat transfer applications was covered by Ali et al[28]. The peristaltic flow of nanofluid through a permeable-walled container was studied by Iqra Shahzadi et al[29]. Akbar[30] conducted an in-depth examination of heat transfer in a peristaltic tube utilizing carbon nanotubes (CNTs). This study produced precise mathematical equations for pressure and velocity gradients as functions of the carbon nanotube volume percentage. These equations are crucial for understanding the dynamics of heat transfer in systems incorporating CNTs. Hayat et al.[31] investigated the peristaltic flow of a water-based fluid incorporating carbon nanotubes and various thermal conductivity models. They found that the presence of carbon nanotubes resulted in a decrease in the velocity profile and an increase in the heat transfer rate at the boundaries, particularly where there was a higher volume fraction of the nanotubes. Additional research on carbon nanotubes (CNTs) is available in the literature.[32-33]

The fluid flow through porous media is driven by Darcy's Law, while the fluid in a free zone is moved by Navier-Stokes equations. In 1967, Beavers and Joseph proposed the boundary condition for the coupled flow motion at the permeable surface. The movement of fluid through permeable walls can enhance mixing within the tube. This can be beneficial in ensuring a uniform distribution of particles or solutes in applications such as chemical reactors or biochemical assays. Permeability of the walls can help in regulating the pressure within the tube. By allowing some fluid to pass through, it can prevent the build-up of excessive pressure that could otherwise damage the system or affect the efficiency of the peristaltic pumping. In recent years, there has been a notable surge in research dedicated to exploring the peristaltic transport of Newtonian and non-Newtonian fluids with permeable walls, with a specific emphasis on diverse geometries. Kothandapani and Srinivas[34] explored the impact of wall characteristics in MHD peristaltic transport including heat transfer and porous media. Rathod and chanakote[35] examined the impact of permeability on the movement of peristaltic in viscous fluid. Akbar et al.[36] studied the copper oxide nano particles analysis with water as a base fluid for peristaltic flow in permeable tube with heat transfer. Asghar et al[37]. examined the Sisko fluid model for peristaltic flow while taking into account mass and heat transfer through the use of a porous medium. The size of the bolus that passes through the oesophagus tends to shrink as the permeability of the porous media increases. The Carreau fluid flow in a rectangular conduit through porous media was studied by Ellahi et al.[38] Their research showed that as the Weissenberg number increases, the velocity also increases. Some important publications on this topic include references.[39-41]

Another aspect of the current model involves *bio-microfluidics*, which focuses on the study of biofluids within micro-scale vessels. In recent decades, bio-microfluidics has garnered considerable attention due to its vast applications in biomedical engineering and sciences. Electro-osmosis is a process where a liquid moves through a capillary or porous material under the influence of an applied electric field. The ion content of the fluid can impact electro-osmotic flow. The transport characteristics of a peristaltic system may be affected by the movement of ions in response to the electric field. In certain cases, the influence of electro-osmotic phenomena on peristaltic transport becomes significant, particularly in microfluidic systems dealing with electrokinetic effects or when electric fields are used to enhance fluid movement. Recently, electro-osmotic flows and peristaltic pumping processes have been the subject of much research, especially for bio-microfluidic applications. Ion mobility in response to an electric field can substantially impact the transport properties of peristaltic systems. Electro-osmosis has the ability to increase flow rate in peristaltic systems. By applying an electric field perpendicular to the flow direction, electro-osmotic flow can be produced alongside peristaltic flow, thereby increasing fluid velocity. The interaction between peristaltic and electro-osmotic actions allows for better control over fluid behaviour. Chakraborty[42] conducted early research on electro-osmotic peristalsis in Newtonian fluids. Building on this work, subsequent research expanded the model to include non-Newtonian effects. Notable studies in this area include those by Tripathi et al[43]. on couple stress fluids, and Ali et al.[44] worked on two-fluid Ellis/Newtonian electro-osmotic peristaltic axisymmetric conduit flows. In a recent study, Khan et al.[45] explored how radiation influences electro-osmosis modulated peristaltic flow within a tapered channel, using Prandtl nanofluid. They discovered that isothermal lines expanded with an increase in the electro-osmotic parameter. Investigation of heat and mass transfer in electroosmotic flow of third order fluid via peristaltic microchannels was discussed by Hussanan et al.[46] Several worthy studies related to the topic are mentioned in.[47-48]

Peristaltic transport of fractional second grade fluids is an advanced topic in fluid mechanics, particularly relevant in bioengineering and industrial applications. A fractional second grade fluid is a type of non-Newtonian fluid characterized by its complex rheological properties, which include both elastic and viscous behaviour that can be described using fractional calculus. This type of fluid model extends the classical second grade fluid model by incorporating fractional derivatives, allowing for a more accurate representation of the fluid's memory effects and time-dependent behaviour. Research in this area typically involves numerical simulations and analytical techniques to solve the governing equations and predict the behaviour of the fluid under various conditions. These studies are important for designing and optimizing systems where peristaltic transport is used, such as in medical devices (e.g., peristaltic pumps) and industrial processes (e.g., transport of slurries and other complex fluids). Understanding the peristaltic transport of fractional second-grade fluids can lead to improved control and efficiency in applications where precise fluid handling is critical. In this context, the research conducted by Channakote et al[49]. Abd-Alla et al[50]. and Tripathi et al.[51-52] , Guo Xiaoyi, and Haitao Qi[53], Hameed et al[54]. is significant. A comprehensive literature review indicates that the study of electro-osmotic forces on bioheat transfer within fractional second-grade (viscoelastic) fluids, particularly in relation to carbon nanotube-based peristaltic transport in biological fluids, has not yet been extensively explored. Incorporating electro-osmotic peristaltic flow with fractional second-grade viscoelastic nanofluids and Carbon nanotubes into engineering and industrial systems offers a range of benefits, including improved fluid control, enhanced heat transfer, and more efficient processing. These applications demonstrate the potential for advanced technologies and innovations across various fields, leveraging the unique properties of nanofluids and CNTs to address complex challenges in modern engineering and industry.

The primary aim of this study is to assess the *significance of incorporating carbon nanotubes (CNTs), specifically single-wall and multi-wall carbon nanotubes, in peristaltic electro-osmotic nanofluid*

propulsion through a permeable wall. In this nanoscale formulation, factors such as heat generation and thermal buoyancy (natural convection) are considered. The findings of this study have practical relevance to nanotechnology applications, such as the use of nanoparticles in the bloodstream for cancer diagnosis, angiography, and angioplasty. Source of inspiration of physiological and biological fluid study may be interpret in the lieu of salient features as:

- To explore the physics of heat transfer on electro-osmotically modulated peristaltic flow of nano-Newtonian nano liquid.
- To model the flow for the symmetric micro channel involving carbon nanotubes, heat generation and thermal buoyancy (natural convection) will be examined by considering permeable wall.
- Physical flow problem after non-dimensional analysis, will be simplified using long wave length and low Reynolds number approximations.
- The analytical expressions are to find for axial velocity, temperature, pressure gradient, pressure rise as well as stream function.
- Impact physical parameter will be explored in the afore mentioned expression.

2. MATHEMATICAL FORMULATION

Let us consider an electro-osmotic-regulated peristaltic flow of within a vertical micro-tube of constant radius d. The carbon nanotubes are suspended in the base fluid to form the nanofluid. The fluid flow is driven by the combined effects of electroosmosis and peristaltic pumping. It is further assumed that the ionic species in the aqueous ionic solution have equal valence, indicating a symmetric solution. The ionic species are set into motion by an external electric field applied across the electric double layer, which in turn carries the adjacent fluid molecules. The fluid flows within a plumb duct, influenced by gravitational force. The physical model is depicted below in Fig. 1. Peristaltic pumping is generated by the propagation of sinusoidal waves along the tube walls, with a constant wave speed c and wavelength λ. A cylindrical coordinate system $(\bar{r}, \bar{z}, \bar{t})$ is adopted. Here, $\bar{r}$ and $\bar{z}$ represent the radial and axial directions, respectively, and $\bar{t}$ signifies time. This coordinate system is found to be more suitable for the mathematical analysis of the flow phenomena.

This research is conducted under certain assumptions, which concurrently act as constraints

- The fractional viscoelastic second grade Reiner-Rivlin differential model is deployed for rheological effects.
- The carbon nanotubes are suspended in the base fluid to prepare the nanofluid.
- An external electric field of unvarying strength E_z in terms of electro-osmotic force is employed on the blood streaming along axial direction (i.e. the positive $\tilde{z}$- direction)
- Caputo's definition of fractional derivatives is used.
- Poisson–Boltzmann equation is simplified via the Debye–Hückel hypothesis, facilitating an exact derivation of the electric potential in the electric double layer (EDL). While this aids the model's mathematical tractability, it may neglect some non-linear dynamics relevant in practical situations.
- The channel walls are preserved at constant temperature T_0.

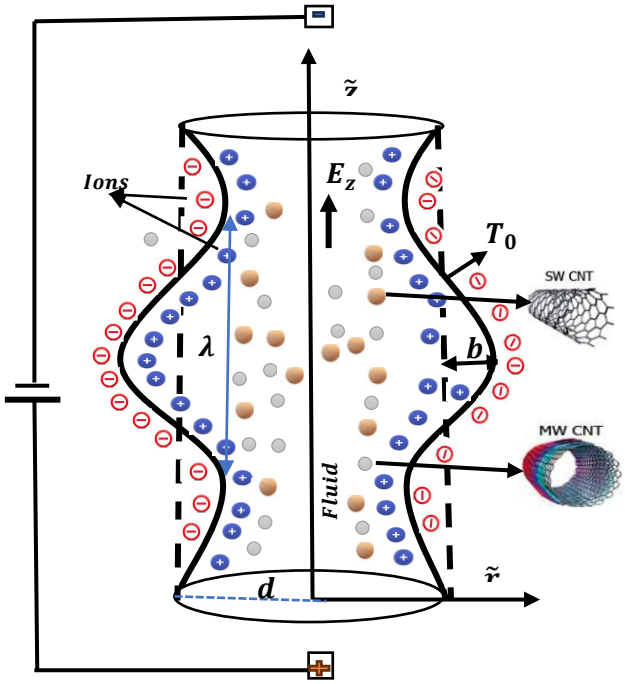

Figure 1. Physical model

The Caputo defines the fractional-order derivative according to Tripathi and Bég [52] as follows:

$$\mathcal{D}^{a_1} f(t) = \frac{1}{\Gamma(n-\alpha)} \int_b^t \frac{f^n(\mathcal{T})}{(t-\mathcal{T})^{a_1+1-n}}\, d\mathcal{T}$$

$$(n-1), Re(a) \leq n, n \in N), \tag{1}$$

Here n is the natural number, $R_e(a) \leq n,$ and a can be a real or complex number.
The Caputo derivatives of t^{β_1} is given by:

$$\mathcal{D}^{\alpha} t^{\beta_1} = \begin{cases} 0 & if \quad (\beta_1 \leq a-1) \\ \frac{\Gamma(\alpha_1+1)}{\Gamma(\alpha_1-\gamma_1+1)} t^{\alpha_1} & if \quad (\beta_1 \geq a-1). \end{cases} \tag{2}$$

The viscoelastic fluid with a fractional second-grade Reiner-Rivlin differential fluid model is represented by the following equation:

$$\tilde{S} = \mu \left(1 + \tilde{\lambda}_1^{\alpha} \frac{\partial^a}{\partial \tilde{t}^a}\right) \dot{\gamma}, \tag{3}$$

Here $\tilde{S}$ is the shear stress, $\tilde{\lambda}_1$ is the physical parameter, $\tilde{t}$ is the time, μ is the dynamic viscosity, $\dot{\gamma}$ represents the shear strain rate, and α is the fractional time derivatives such that $(0 < a \leq 1)$. When $a = 1$, the model simplifies to the conventional second-grade model, and setting $\lambda_1 = 0$ leads to the classical Newtonian (Navier-Stokes) case.
Compliant motion is mathematically represented as the contraction and relaxation of the distensible micro-tube wall.

$$h = 1 + \epsilon \cos(2\pi z) \tag{4}$$

The following expression can govern the flow:
Continuity equation:

$$\frac{\partial \tilde{u}}{\partial \tilde{r}} + \frac{\tilde{u}}{\tilde{r}} + \frac{\partial \tilde{w}}{\partial \tilde{z}} = 0, \tag{5}$$

Momentum equation in the axial direction:

$$\rho_{nf}\left(\frac{\partial \tilde{w}}{\partial \tilde{t}} + \tilde{u}\,\frac{\partial \tilde{w}}{\partial \tilde{r}} + \tilde{w}\frac{\partial \tilde{w}}{\partial \tilde{z}}\right) = -\frac{\partial \tilde{p}}{\partial \tilde{z}} + \mu_{nf}\left(1 + \lambda_1^{\alpha}\frac{\partial^{\alpha}}{\partial \tilde{t}^{\alpha}}\right)\left[\frac{1}{\tilde{r}}\frac{\partial}{\partial r}\left(\tilde{r}\frac{\partial \tilde{W}}{\partial \tilde{r}}\right) + \frac{\partial^2 \tilde{w}}{\partial \tilde{z}^2}\right] + (\rho v)_{nf} g\left(\tilde{T} - \tilde{T}_0\right) + \rho_e E_{\tilde{z}} \Big\} \tag{6}$$

Momentum equation in the radial direction:

$$\rho_{nf}\left(\frac{\partial \tilde{u}}{\partial \tilde{t}} + \tilde{u}\,\frac{\partial \tilde{u}}{\partial \tilde{r}} + \tilde{w}\frac{\partial \tilde{u}}{\partial \tilde{z}}\right) = -\frac{\partial \tilde{p}}{\partial \tilde{r}} + \mu_{nf}\left(1 + \tilde{\lambda}_1^{\alpha}\frac{\partial^{\alpha}}{\partial \tilde{t}^{\alpha}}\right)\left[\frac{1}{\tilde{r}}\frac{\partial}{\partial \tilde{r}}\left(\tilde{r}\frac{\partial \tilde{u}}{\partial \tilde{r}}\right) + \frac{\partial^2 \tilde{u}}{\partial \tilde{z}^2}\right] + \rho_e E_r \tag{7}$$

Energy equation:

$$\left(\rho c_p\right)_{nf}\left(\frac{\partial \tilde{T}}{\partial \tilde{t}} + \tilde{u}\,\frac{\partial \tilde{T}}{\partial \tilde{r}} + \tilde{w}\frac{\partial \tilde{T}}{\partial \tilde{z}}\right) = k_{nf}\left(\frac{\partial^2 \tilde{T}}{\partial \tilde{r}^2} + \frac{1}{\tilde{r}}\frac{\partial \tilde{T}}{\partial \tilde{r}} + \frac{\partial^2 \tilde{T}}{\partial \tilde{z}^2}\right) + Q_0, \tag{8}$$

In Eqns. (6-8), $\tilde{u}$ and $\tilde{w}$ are the velocity components in the radial and axial direction respectively, E_r and E_z represents the electric body force in the radial and axial co-ordinates, μ_{nf} is the viscosity of the carbon nano tube (CNT)-ionic nano-liquid, ρ_{nf} is the effective density. $\tilde{T}$ represents the temperature, k_{nf} represents the nanofluid thermal conductivity, Q_0 is the parameter of heat source. $\left(\rho c_p\right)_{nf}$ represents the specific heat of the nano liquid. $(\rho v)_{nf}$ is the thermal expansion coefficient of the nano fluid.

The basic mixing rule is used to calculate the effective density (ρ_{nf}), specific heat (c_{pnf}), and thermal expansion coefficient (α_{nf}) of the Carbon nanotube (CNTs)-aqueous ionic nanofluid. Then, using the Maxwell model and Brinkman's relations, the viscosity (μ_{nf}) and thermal conductivity (k_{nf}) of the nanofluid are computed. The results are presented as follows, respectively.

$$\left.\begin{aligned} \rho_{nf} &= (1-\phi)\rho_f + \phi\rho_{CNT}, \mu_{nf} = \frac{\mu_f}{(1-\phi)^{2.5}} \\ \left(\rho c_p\right)_{nf} &= (1-\phi)\left(\rho c_p\right)_f + \phi\left(\rho c_p\right)_f, a_{nf} = \frac{k_{nf}}{\left(\rho c_p\right)_{nf}} \\ (\rho v)_{nf} &= (1-\phi)(\rho v)_f + \phi(\rho v)_{CNT}, \\ k_{nf} &= k_f\left(\frac{(1-\phi)+\frac{2\phi k_{CNT}}{k_{CNT}-k_f}\log\left(\frac{k_{CNT}+k_f}{2k_f}\right)}{(1-\phi)+\frac{2\phi k_f}{k_{CNT}-k_f}\log\left(\frac{k_{CNT}+k_f}{2k_f}\right)}\right) \end{aligned}\right\}, \tag{9}$$

The variables ϕ, subscript f, and superscript p denote the volume fraction of carbon nanotubes (CNTs), the base fluids characteristics, and the solid particle properties, respectively. The electric potential distribution in the aqueous ionic nanofluid is described by the Poisson-Boltzmann equation as follows:

$$\nabla^2\tilde{\Phi} = \frac{1}{\tilde{r}}\frac{\partial}{\partial r}\left(\tilde{r}\frac{\partial \tilde{\Phi}}{\partial \tilde{r}}\right) = \frac{\rho_e}{\varepsilon_r \varepsilon_0}. \tag{10}$$

Here, ∇^2 is the Laplacian operator, ϕ is the electric potential, ρ_e is the charge density, relative ε_r is the permittivity of the medium, ε_0 is the permittivity of the vacuum and electric number density in terms of the number cations and the anions are indicated by, $n^+$and n^-, respectively.

$$\rho_e = ez(n^+ - n^-). \tag{11}$$

To analyse the fluid dynamics of the peristaltic moving boundary problem in a steady state, it is essential to convert the coordinates from the laboratory frame$(\tilde{z}, \tilde{r})$ to a wave frame of reference (z, r). The transformation equations for the coordinates can be expressed as follows:

$$\tilde{r} = \bar{r}, \tilde{z} = \tilde{z} - c\tilde{t}, \tilde{u} = u, \tilde{w} = w - c, \tilde{p}(\tilde{z}, \tilde{r}, \tilde{t}) = \tilde{p}\left(\tilde{z}, \tilde{r}, \tilde{T}\right). \tag{12}$$

Non-dimensional analysis is a useful method for simplifying the flow problem under study. Throughout this procedure, dimensionless scaling variables are introduced and defined as follows:

$$\left.\begin{gathered} m=\sqrt{\frac{2n_0\,e^2z^2d^2}{\varepsilon_0\varepsilon_r k_f\tilde{T}_{avg}}}=\frac{d}{\lambda_d}, U_{Hs}=\frac{E_z\varepsilon_r\,k_f\tilde{T}_{avg}\varepsilon_0}{ez\mu_f c}, p=\frac{a^2\tilde{P}}{c\lambda\,\mu}, \theta=\frac{\tilde{T}-T_0}{T_0}, t=\frac{c\tilde{t}}{\lambda}, \\ \beta_1=\frac{Q_0d^2}{T_0k_f}, \Phi=\frac{ez\tilde{\Phi}}{k_fT_{avg}}, w=\frac{\tilde{w}}{c}, u=\frac{\tilde{u}}{c\delta}, z=\frac{\tilde{z}}{\lambda}, r=\frac{\tilde{r}}{d}, \delta=\frac{d}{\lambda}, Re=\frac{\rho_f\,c\,d}{\mu_f}, L=\frac{(\rho\nu)_{nf}}{(\rho\nu)_f} \\ pr=\frac{c_p\mu}{k}\ \epsilon=\frac{b}{d}, h=\frac{\tilde{h}}{d}, \lambda_1=\frac{c\tilde{\lambda}_1}{\lambda}, p=\frac{\tilde{p}d^2}{\mu\,c\,\lambda}, Gr=\frac{\rho_f g\gamma_f d^2T_0}{\mu_f c}, \end{gathered}\right\}. \tag{13}$$

Next, by employing the lubrication linearization theory for long wavelengths and low Reynolds numbers, we arrive at the following simplified equations:

$$\frac{1}{r}\frac{\partial(r\,u)}{\partial r}+\frac{\partial w}{\partial z}=0, \tag{14}$$

$$\frac{\partial p}{\partial r}=0, \tag{15}$$

$$\frac{\partial p}{\partial z}=\frac{1}{(1-\phi)^{2.5}}\left\{1+\lambda_1^{\alpha}\frac{\partial^{\alpha}}{\partial\tilde{t}^{\alpha}}\right\}\left(\frac{\partial^2 w}{\partial r^2}+\frac{1}{r}\frac{\partial w}{\partial r}\right)+\frac{1}{r}\frac{\partial}{\partial r}\left(r\left(\frac{\partial\Phi}{\partial r}\right)\right)U_{Hs}+GrL\,\theta \tag{16}$$

$$\left(\frac{\partial^2\theta}{\partial r^2}+\frac{1}{r}\frac{\partial\theta}{\partial r}\right)+\beta_1\left(\frac{k_f}{k_{nf}}\right)=0, \tag{17}$$

$$\frac{1}{r}\frac{\partial}{\partial r}\left(r\left(\frac{\partial\Phi}{\partial r}\right)\right)=m^2\left(\frac{\mathrm{n}^+-\mathrm{n}^-}{2}\right), \tag{18}$$

Here U_{HS}, is electro-osmotic Helmholtz-Smoluchowski velocity, β_1 is source/sink, in fluid dynamics, the concept of a *source or sink* is used to describe regions where heat is either added to or removed from a system. These terms help in understanding and modelling various fluid flow situations. Gr*, is Grashoff number, the* Grashoff number quantifies the strength of buoyancy forces in a fluid. Buoyancy forces arise due to density differences caused by temperature variations, m*,* is Debye-Huckle parameter θ, is temperature, ϕ is nanoparticle volume fraction of carbon nanotube (CNTs), and λ_1, is second grade viscoelastic material parameter, Second-grade viscoelastic materials are a type of non-Newtonian fluid that exhibits more complex behaviour than simple Newtonian fluids and when the zeta potential is low, the linearized Boltzmann distribution may be used to estimate the electric potential in a fluid medium. This approach gives a precise evaluation of the ionic species' local distribution without making the flow problem more difficult to solve. The resultant electric potential is usually less than or equal to 25 mV, as is the case with most electrolyte solutions.

$$n^{\pm}=e^{\mp\Phi} \tag{19}$$

Following Tripathi et al. [43], we obtain the Poisson-Boltzmann equation by using Eq. (19) in Eq. (16) as follows:

$$\frac{1}{r}\frac{\partial}{\partial r}\left(r\left(\frac{\partial\Phi}{\partial r}\right)\right)=m^2\sinh(\Phi)\,. \tag{20}$$

Using the approximation that $\sinh(\Phi)\ \approx\ \Phi$, Eqn. (20) is further simplified by applying Debye-Huckel theory, as suggested by Tripathi et al. [43].

$$\frac{1}{r}\frac{\partial}{\partial r}\left(r\left(\frac{\partial\Phi}{\partial r}\right)\right)=m^2\Phi. \tag{21}$$

The dimensionless no-slip boundary conditions for temperature, velocity, and electric potential applied along the tube wall are given by the following equations.

$$\frac{\partial w}{\partial r} = 0 \; at \; r = 0, \; w = -1 - \frac{\sqrt{Da}}{\eta}\frac{\partial w}{\partial r} \; at \; r = h, \tag{22}$$

$$\frac{\partial \theta}{\partial r} = 0 \; at \; r = 0, \; \theta = 0, \; h = 1 + \epsilon \cos(2\pi z)\,, \tag{23}$$

$$\frac{\partial \Phi}{\partial \tilde{r}} = 0 \text{ at } r = 0 \text{ and } \Phi = 1 \text{ at } r = h(z). \tag{24}$$

3. EXACT SOLUTIONS

Employing the boundary conditions of Eq. (24) to solve the Eq. (21), we obtain the electrical potential function as:

$$\Phi = \frac{I_0(m,r)}{I_0(m,h)}\,. \tag{25}$$

Solving Eqns. (16) and (17), along with the boundary conditions (22) and (23), the expression for velocity and temperature are:

$$w = \frac{1}{64A\eta I_0(mh)k_{nf}\mu_f}(GrL\big(4\sqrt{Da}h^3 + (3h^4 - 4h^2r^2 + r^4)\eta\big)I_0(hm)k_f\beta_1\mu_{nf} + 16k_{nf}(-4A\eta I_0(h\,m)\mu_f + \big(p\big(-2\sqrt{Da}h - h^2\eta\big)I_0(hm) + 4\big(-\eta I_0(h\,m) + \eta I_0(mr) + \sqrt{Da}\,mI_1(hm)\big)U_{Hs}\big)\mu_{nf}\big)). \tag{26}$$

Here $I_0\,(x)$ and $I_1(x)$ are modified Bessel function of the first kind defined as.

$$I_j(x) = \sum_{i=0}^{\infty}\frac{1}{i!\Gamma(i+j+1)}\left(\frac{x}{2}\right)^{2i+j} \tag{27}$$

$$\theta = \frac{\beta_1\, k_f}{4\, k_{\mathrm{nf}}}(h^2 - r^2)\,. \tag{28}$$

We use the volumetric flow rate in the moving frame to calculate the pressure gradient, which yields the following equation.

$Q = \int_0^h 2\,r\,w\,dr$, in consequences as a result of Eqn. (26), becomes:

$$Q = -h^2 + \frac{\mathrm{h}\Big(-6h^2p(4\sqrt{Da}+h\eta)+48\Big(-h\eta+\frac{(\sqrt{Da}hm^2+2\eta)I_1(hm)}{mI_0(\,hm)}\Big)U_{Hs}+\frac{Gr\,h^4L(\sqrt{Da}+h\eta)k_f\,\beta_1}{\mathrm{k_{nf}}}\Big)\mu_{nf}}{48A\,\eta\mu_{nf}}\,. \tag{29}$$

The time-averaged flow rate Q is then computed as:

$$\tilde{Q} = Q + \frac{1}{2}\Big(1 + \frac{\epsilon^2}{2}\Big). \tag{30}$$

The axial pressure gradient is calculated as:

$$\frac{dp}{dz} = \frac{48\Big(-h\eta+\frac{(\sqrt{Da}hm^2+2\eta)I_1(hm)}{mI_0(hm)}\Big)U_{Hs}+\frac{GrLh^5L(3\sqrt{Da}+h\eta)k_f\beta_1}{k_{nf}}-\frac{48\,A(h^2+\tilde{Q})\eta\mu_{nf}}{\mu_{nf}}}{6\,h^3(4\sqrt{Da}+\mathrm{h}\eta)}. \tag{31}$$

Were, $A = \left(1 + \lambda^{\alpha}\left(\frac{t^{\alpha}}{\Gamma(1-\alpha)}\right)\right)$

The pressure rise Δp and friction force F_{λ} are, respectively, given by

$$\Delta p = \int_0^1 \frac{\partial p}{\partial z} dz \,, \tag{32}$$

$$F_\lambda = \int_0^1 \left(-h^2 \frac{\partial p}{\partial z}\right) dz \,. \tag{33}$$

The expression for resultant stream function can be obtained by the following equations:

$$w = -\frac{1}{r}\frac{\partial \psi}{\partial z}, w = \frac{1}{r}\frac{\partial \psi}{\partial r} \;\; at \; r = h \,. \tag{34}$$

4. GRAPHICAL RESULTS AND DISCUSSION:

In **Figure 2** and **Table 1**, information on the effective heat conductivity of nanofluids with single- and multi-walled carbon nanotubes (SWCNT and MWCNT) is provided.

Table 1. Thermal properties of the base fluid (water) and CNTs:

Fluid phase (water)		Cu	SWCNT	MWCNT
c_p	4.179	385	425	796
ρ	997.1	8,933	2,600	1,600
k	0.613	400	6,600	3,000
Pr	6.9			

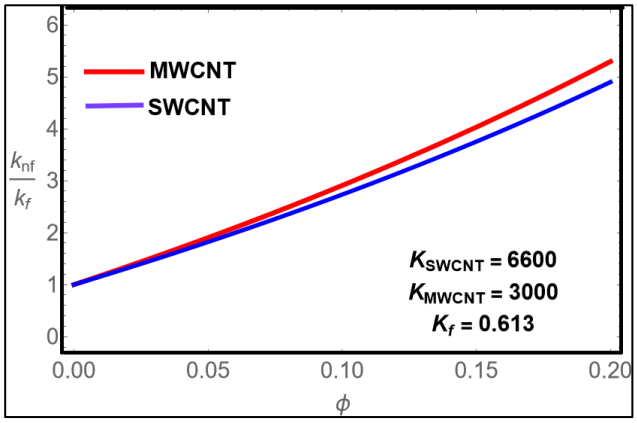

Figure 2. Effective thermal conductivity of the Nano fluid

Compared to single walled carbon nanotube ($SWCNTs$), multiwalled carbon nanotube($MWCNTs$) notably has a greater thermal conductivity. Additionally, the distinction between SWCNT and MWCNT is more noticeable when the nanofluid's volume fraction rises ($\phi > 0$). The effects of important Multiphysics factors on temperature, axial pressure gradient, pumping, and trapping characteristics for the regime are then discussed. Analytical solutions using physically feasible data have been computed as graphs using Mathematica software.

4.1 Velocity profiles:

The primary purpose of this section is to analyse the impact of pertinent parameters, Helmholtz-Smoluchowski velocity parameters U_{Hs}, electro-osmotic parameter (m), Darcy numbers (Da).

Source/sink parameter,(β_1) Grashoff number (Gr) on velocity (w). For this purpose, Figures (3a-3f) are sketched to measure the features of all parameters. In particular, the variations of all parameters are examined. The magnitude of the physical parameters for velocity profile are chosen to match the problems physical circumstances.

Figure 3(a) shows the axial velocity distribution for different Helmholtz-Smoluchowski velocity parameters. For both single walled carbon nanotube (SWCNT/water) and Multiwalled carbon nanotube multiwalled carbon nanotube (MWCNT/water) ionic nanofluids, it is observed that an increase in positive U_{Hs} velocity causes an increase in axial velocity in the micro-tube's core zone (around the centreline, $r = 0$), while a definite deceleration is computed in the peripheral zone, or close to the tube's boundaries ($r = -1,1$). As stated in equation (13), the Helmholtz-Smoluchowski parameter is $U_{Hs} = \frac{E_z \varepsilon_r \, k_f \tilde{T}_{avg} \varepsilon_0}{ez\mu_f c}$ and is proportional to the axial electrical field, E_z. This parameter appears in the dimensionless axial momentum conservation equation (16) as the electro-osmotic body force, $+\frac{1}{r}\frac{\partial}{\partial r}\left(r\left(\frac{\partial \Phi}{\partial r}\right)\right)U_{Hs}$. The fact that U_{HS} is directly proportional to E_z implies that by increasing the electric field, the electroosmotic flow is enhanced, leading to a stronger axial flow in the core zone. This relationship highlights the role of the electric field in controlling the flow dynamics of ionic nanofluids.

Figure 3(b) shows how the electro-osmotic parameter (m) affects the axial velocity profile. A notable slowing is noticed near the centre of the micro-tube with an upsurge in the electroosmotic parameter, m, which corresponds to a lower Debye length. This happens because a shorter Debye length implies that the electroosmotic effects are more localized near the boundaries, reducing their influence in the core region. As a result, the flow in the core zone slows down since it experiences less electroosmotic push. At the highest value of $m = 4$, the velocity profile in the core zone becomes a reversed parabola, indicating a more pronounced deceleration in the center. This is a direct consequence of the strong electroosmotic effects near the walls (due to the short Debye length), which dominate the flow behavior and reduce the velocity in the core. The core profile for $m = 2, 3, 4$ and the trend is consistent slowing down across the micro-tube, i.e., for all radial locations. The parameter m as noted is inversely related to the electric double layer (EDL). Figure 3(c) shows the behaviour of the velocity profile with varying Darcy numbers (Da). There is a progressive reduction in the axial flow velocity with increasing Da. This suggests that as the permeability of the walls increases (higher Da), the fluid can seep more easily into the porous walls, reducing the effective flow within the core of the tube. Essentially, fluid is being diverted into the porous walls, which decreases the axial flow velocity in the main channel. Additionally, as Da increases, the fluid discovers more pathways through the porous medium, effectively reducing the available space (or gap) for fluid to flow through the central region of the tube. Consequently, the axial velocity decreases as the flow are distributed between the porous medium and the main channel.

Figure 3(d) depicts the effect of the heat source parameter, β_1, on the velocity distribution along the radial span of the microtube. A significant increase in axial velocity in the core zone is observed as heat generation rises (positive β_1). The thermal energy added to the peristaltic regime energizes the flow through the $+\beta_1\left(\frac{k_f}{k_{nf}}\right)$ term in the energy equation (17). The peristaltic micro-pump may develop a thermal hotspot connected to heat production, potentially serving as a source of heat injection into the regime. Despite the high acceleration in the core zone due to momentum redistribution, the periphery zone near the microtube walls decelerates. Figure 3(e) illustrates the effect of various CNT volume fractions (ϕ) on the velocity distribution. As the CNT doping in the aqueous ionic nanofluid increases, there is a significant flow acceleration throughout the microtube zone, evidenced by the notable velocity increases in both SWCNT/water and MWCNT/water as (ϕ) rises. The suspension of additional CNTs in the ionic nanofluid reduces the mixture's effective viscosity, thereby lowering viscous resistance and

causing flow acceleration. These flow characteristics, due to the reduction in viscosity and the associated acceleration of flow, validate the use of carbon nanotube CNTs in enhancing fluid performance. Increased carbon nanotube (CNTs) volume fractions accelerate flow, enhancing peristaltic pumping efficiency. CNTs reduce viscosity, allowing more effective fluid pumping with less energy loss. This is advantageous for applications needing precise fluid control, like biomedical devices and microfluidic systems.

Figure 3(f) illustrates the response in axial fluid velocity and thermal Grashof number (Gr). It is observed that across the entire micro-tube span, but primarily in the core (middle) region of the micro-tube, the velocity profile increases consistently with increment in thermal Grashof number for both single walled carbon nanotube *(SWCNT/water*) and multiwalled carbon nanotube *(MWCNT/water)*. A higher Grashof number (Gr) signifies a stronger thermal buoyancy effect compared to viscous force. The thermal buoyancy body force, $+GrL\,\theta$ in Eqn. (17) is amplified and this mobilizes strong natural convection currents which intensify and accelerate the flow. For the case $Gr = 0$, thermal buoyancy vanishes and forced convection is present (de-coupling of momentum (17) and energy (18) equations). The physical motivation behind the graph in Figure 3(f) shows that increasing the thermal Grashof number enhances thermal buoyancy, which boosts natural convection currents and accelerates fluid flow in the micro-tube. Higher Grashof numbers lead to increased axial velocities and better heat transfer, particularly in the core region. This highlights the significant impact of buoyancy forces on flow and thermal performance, further enhanced by carbon nanotube CNTs.

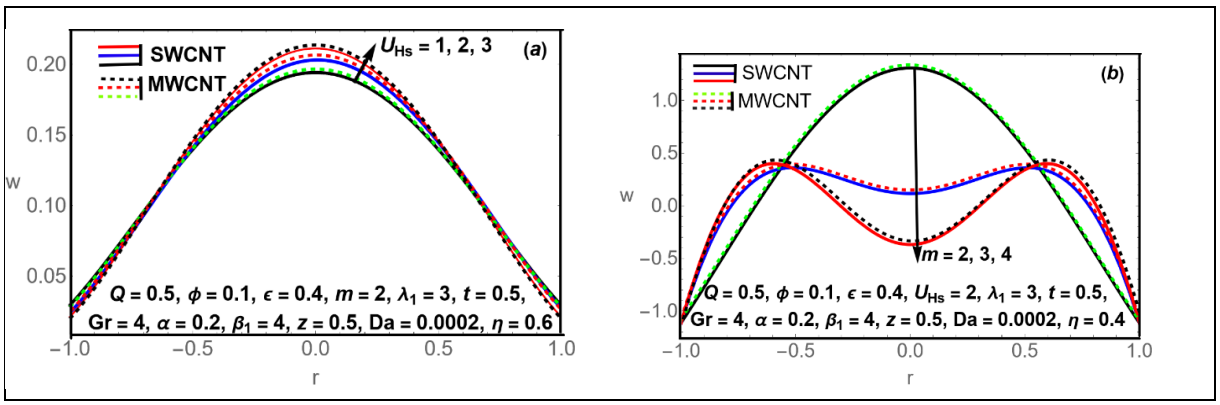

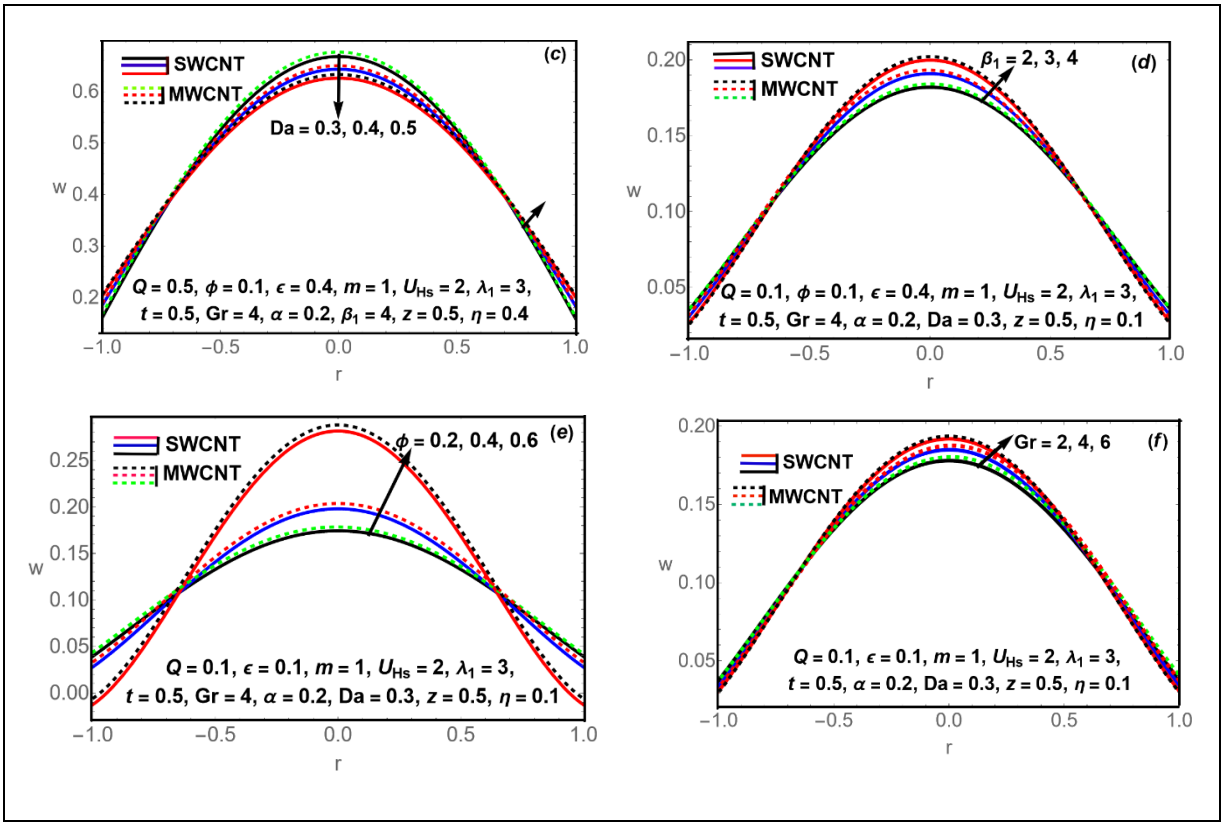

Figure 3: Axial velocity distribution with variation in (a) Helmholtz-Smoluchowski velocity parameter (U_{Hs}), (b) electro-osmotic parameter (m),(c) Darcy number Da, (d) thermal source/sink parameter (β_1), (e) carbon nanotube (CNT) volume fraction (ϕ).

4.2 Temperature profiles:

Understanding the impact of the heat source/sink parameter and CNT volume fraction is important for controlling the temperature in microfluidic and biomedical systems. For example, in drug delivery applications, maintaining precise temperature control can be crucial for the stability of therapeutic agents.

The impact of the heat source/sink parameter, denoted as β_1 and the carbon nanotube (CNTs) volume fraction, ϕ, on the temperature profiles across the microtube are visualized in **Figures** 4(a) and 4(b). The temperature profile increases with an increase in the values of the heat source parameter β_1 at all radial locations. The injection of heat (thermal energy) clearly accentuates the temperature magnitudes in the porous peristaltic regime. This implies that the injection of heat raises the overall temperature of the fluid, making the fluid warmer as more thermal energy is introduced. The effect is observed throughout the microtube, from the centre (core zone) to the edges (peripheral zones). While the case of heat sink $(\beta_1 < 0)$ has not been plotted, it will induce the opposite response i.e. cooling in the microtube in both the core and peripheral zones. Conversely, the temperature profile decreases with an increase in the CNT volume fraction ϕ. It is clearly observed that the heat produced by the heat source is rapidly transferred to the walls due to the addition of CNTs, resulting in a decline in fluid temperature. The rapid decrease in fluid temperature is facilitated by the high thermal conductivity of CNTs.

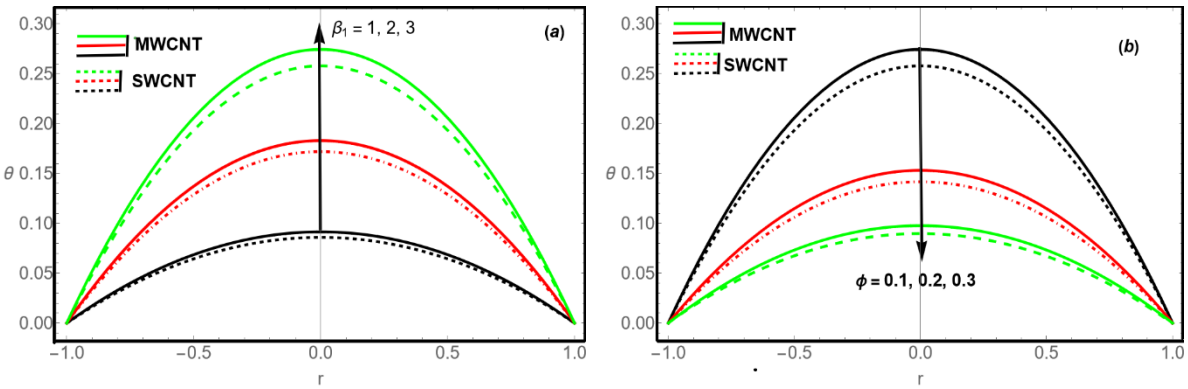

Figure 4(a) Impact of source / sink parameter β_1 on θ Figure 4(b) Impact of CNT volume fraction ϕ on θ [for fixed values of other parameters $(\epsilon = 0.1, z = 0.5,)$]

4.3. Axial Pressure Gradients:

The pressure gradient in peristaltic flow is crucial for determining the direction, rate, and efficiency of fluid transport. It influences the mechanical interaction between the fluid and the conduit walls, ensuring that the system can adapt to various conditions and maintain optimal performance. Figures 5a-b illustrate the pressure gradient plotted for various values of m and U_{Hs}, and at different axial (z) coordinates. Each figure corresponds to a different axial coordinate, showcasing how the pressure gradient changes along the length of the conduit for different values of m and U_{Hs}. The pressure gradient response to an increase in the inverse electrical double layer (EDL) thickness, represented by the Debye-Hückel parameter $(m = a/\lambda d)$, is depicted in **Figure** 5(a). It has been observed that the pressure gradient elevated with the increasing Debye-Hückel parameter, i.e., with decreasing characteristic thickness of EDL, and the decreasing characteristic thickness of EDL can reduce the negative pressure gradient. This finding indicates that as the typical thickness of the EDL decreases, a negative pressure gradient is likely to occur. **Figure 5(b)** shows that the pressure gradient increases steadily as the Helmholtz-Smoluchowski velocity (U_{Hs}) rises, which is proportional to the external axial electric field. Furthermore, the negative pressure gradient may be mitigated by an intensifying external electric field. The pressure gradient for various values of Darcy number (Da) and CNT volume fraction, (ϕ) is plotted in **Figures** 5(c-d). From the **Figure** 5(c), it is evident that the magnitude of the pressure gradient increases with higher values of (Da). In another words, the electro-osmotic inverse EDL parameter m and Helmholtz-Smoluchowski velocity (U_{Hs}) the trend is maintained across all axial location z. Also, the Darcy number positively influences the axial pressure gradient. Furthermore, the highest-pressure gradient is observed around $z = 0.5$ the midpoint of the microtube length. This indicates that while flow is sub-optimal at the entry $z = 0$ and exit $z = 1$sites, it is optimal at the centre axial position. Additionally, it is noted that the pressure gradient for multi-walled carbon nanotubes (MWCNT) is somewhat higher than that for single-walled carbon nanotubes (SWCNT). **Figure** 5(d) demonstrates that a constant reduction in the axial pressure gradient is produced by increasing the CNT volume fraction (ϕ), or by further doping with SWCNTs or MWCNTs. Consequently, with a higher fraction of CNTs in the peristaltic aqueous ionic Nano fluid flow, the axial pressure gradient exhibits an inverse reaction to increasing velocity magnitudes, as previously estimated. Furthermore, it is observed that, in comparison to SWCNTs, MWCNTs generate a slightly higher axial pressure gradient $\frac{dp}{dz}$. **Figure** 5(e) is portrayed to get the influence of (λ_1) on the pressure gradient. We clearly see in this figure that pressure gradient diminishes for rising values of local parameter λ_1. This means that higher values of λ_1 result in less resistance to flow, thereby decreasing the pressure needed to drive the fluid through the

tube. The impact of the Grashoff number, denoted as (Gr) on the axial pressure gradient $\frac{dp}{dz}$ has been shown through **Figure** 5(f). It is seen from the figure that for $z \in [0,0.2]$ and $z \in [0.8,1]$ the pressure gradient is small, larger pressure gradient occurs for $z \in [0.3,0.7]$; moreover, it is noted that with an increase in Gr the pressure gradient increases. Furthermore, it is noted that the pressure gradient for (SWCNT) is slightly lesser than that of (MWCNT). Increasing the Grashof number leads to a higher axial pressure gradient due to stronger buoyancy-driven convection, especially in the central regions of the microtube. SWCNTs show a slightly lower pressure gradient than MWCNTs, reflecting differences in flow resistance. This information is essential for optimizing fluid flow and heat transfer in systems involving thermal effects and CNT suspensions.

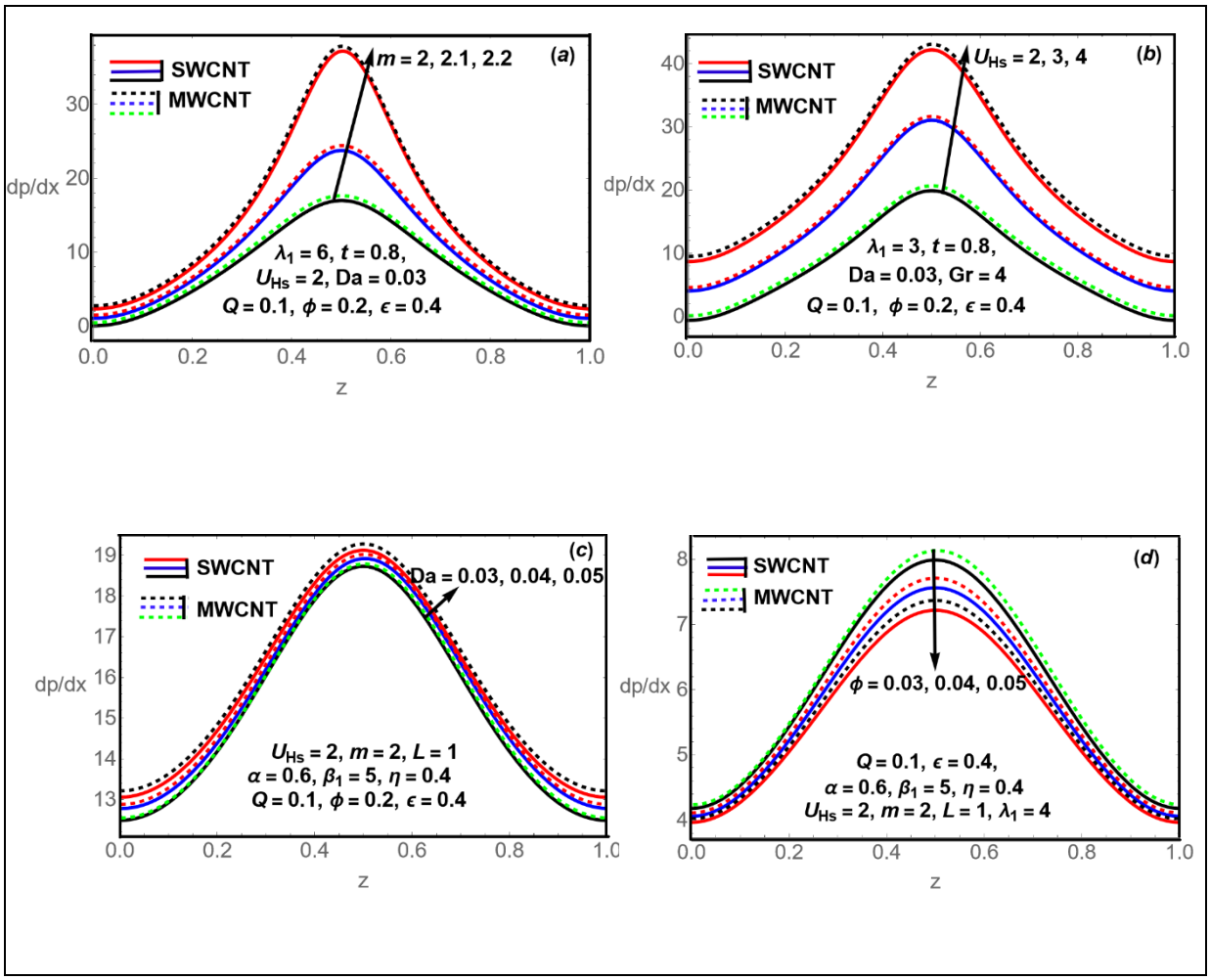

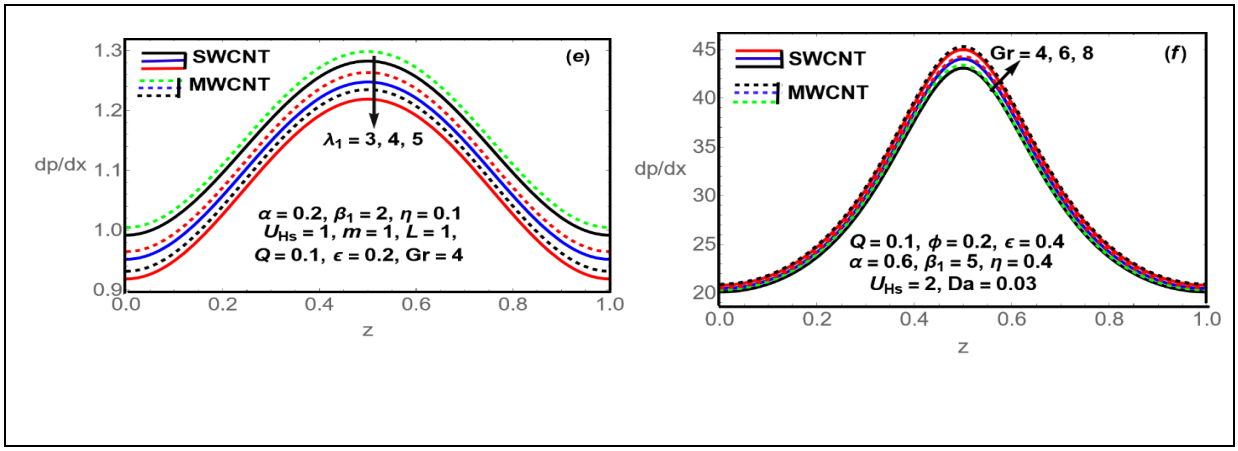

Figure 5: Axial pressure gradient distributions with variation in (a), electro-osmotic parameter (m), (b) Helmholtz-Smoluchowski parameter U_{Hs}, (c) Darcy number (Da), (d) the CNT volume fraction (ϕ), (e), material constant λ_1, (f) Grashoff number (Gr), and for fixed values of other parameters

4.4 Pumping Characteristics:

Peristaltic flow is a highly effective technique for moving liquids, as demonstrated in bio-inspired peristaltic micro pumps and natural processes such as human swallowing and digestion. The effective movement of waste materials and nutrients is ensured by the pressure increase. This pressure rise in peristaltic flow is crucial because it facilitates fluid transportation, mixing, metering, dispensing, contamination control, and gentle fluid handling. It is also relevant in various industrial and biological processes. Pressure rise Δp is plotted against Q in **Figures** 6(a–c), for different values of the Helmholtz-Smoluchowski velocity (U_{Hs}) and Debye-Huckel parameter i.e. inverse EDL parameter (m), and Grashoff number (Gr). It is found that in the retrograde pumping zone $(\Delta p > 0, Q < 0)$, the peristaltic pumping region $(\Delta p > 0, Q > 0)$ and also the augmented pumping zone $(\Delta p < 0, Q > 0)$, increases with increasing the Helmholtz-Smoluchowski velocity (U_{HS}), inverse EDL parameter (m) and Grashoff number (Gr). In Figure 6(d) we observed that the peristaltic pumping rate of ionic nanofluid increases with the elevation in heat source parameter, (β_1) in all the three pumping regions. Figure 6(e) illustrates the variation of pressure rise with the average volume flow rate for different values of the second-grade material parameter (λ_1). The figure demonstrates that the magnitudes of the axial pressure gradient decrease with higher values of (λ_1). This reduction occurs because the fractional viscoelastic fluid takes longer to relax after the removal of stress. Additionally, the pressure increases magnitudes (Δp) for multiwalled carbon nano tube MWCNTs are consistently higher than those for single walled carbon nano tube SWCNTs

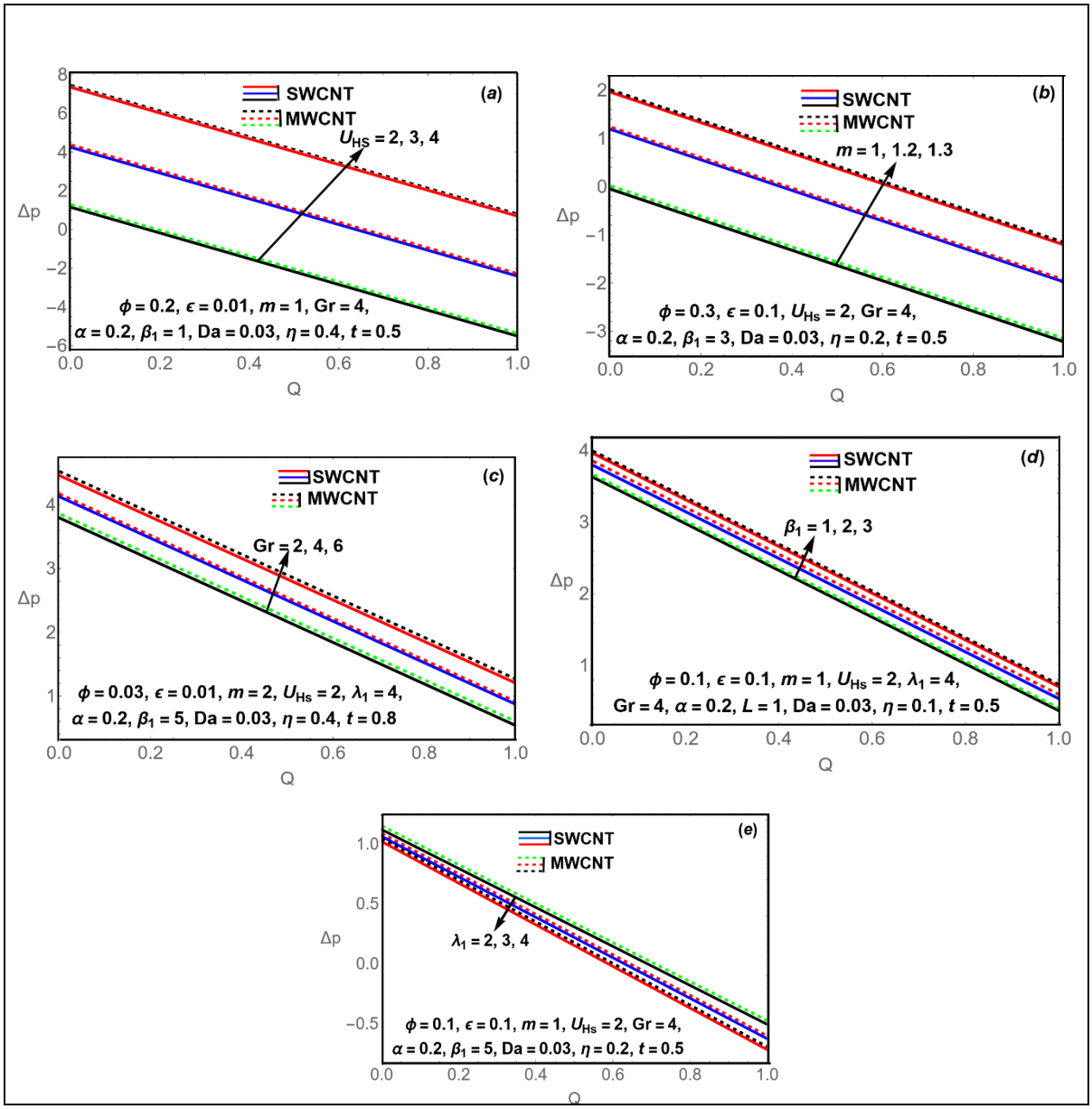

Figure 6: Pressure rise versus mean flow rate Q with variation in (a), Helmholtz-Smoluchowski parameter (U_{Hs}) (b) electro-osmotic parameter (m), (c) Grashoff number Gr (d) Source sink parameter (β_1), (e) viscoelastic material parameter(λ_1), and for fixed values of other parameters.

4.5 Trapping Characteristics (Bolus Dynamics):

By computing streamline distributions, the trapping phenomenon can be investigated in greater detail, providing insight into the formation of fluid zones (boluses) within the peristaltic regime and the movement of matter in micro-peristaltic pump systems. This includes the transport of waste materials, cells, robotic ionic fluids, and other substances. This analysis is particularly relevant in biological and biomedical applications, where regulated substance transit is essential. It also has applications in tissue engineering and cell sorting. Understanding bolus dynamics can be used to optimize the controlled manipulation of substances and enhance mixing in microfluidic devices.

The streamline patterns for single walled carbon nano tube $SWCNT$ and multiwalled carbon nano tube $MWCNT$ flow against various electro-osmotic parameter values (m) and Helmholtz-Smoluchowski

velocity parameter values (U_{Hs}) are displayed in Figs. 7-9. We also take into account the differences in the thermal conductivity of single walled carbon nano tube SWCNT (K_{SWCNT}) for the base row and multiwalled carbon nano tube $MWCNT$ (K_{MWCNT}) for the top row of streamlines in each of the three plots. The streamline pattern is displayed in Figure. 7 for various values of the electro-osmotic parameter (m), as well as the thermal conductivity of $MWCNT$ (K_{MWCNT}) for the top row and $SWCNT$ (K_{SWCNT}) for the base row. The trapped bolus inside the streamlines indicates that the fluid is carried by peristaltic action with the help of permeable walls. A rising electro-osmotic parameter (m) enhances the amplitude of both the top and lower boluses in a dual bolus structure that is generated. When comparing the $SWCNT$ (K_{SWCNT}) to the $MWCNT$ (K_{MWCNT}), a somewhat bigger bolus structure is seen.

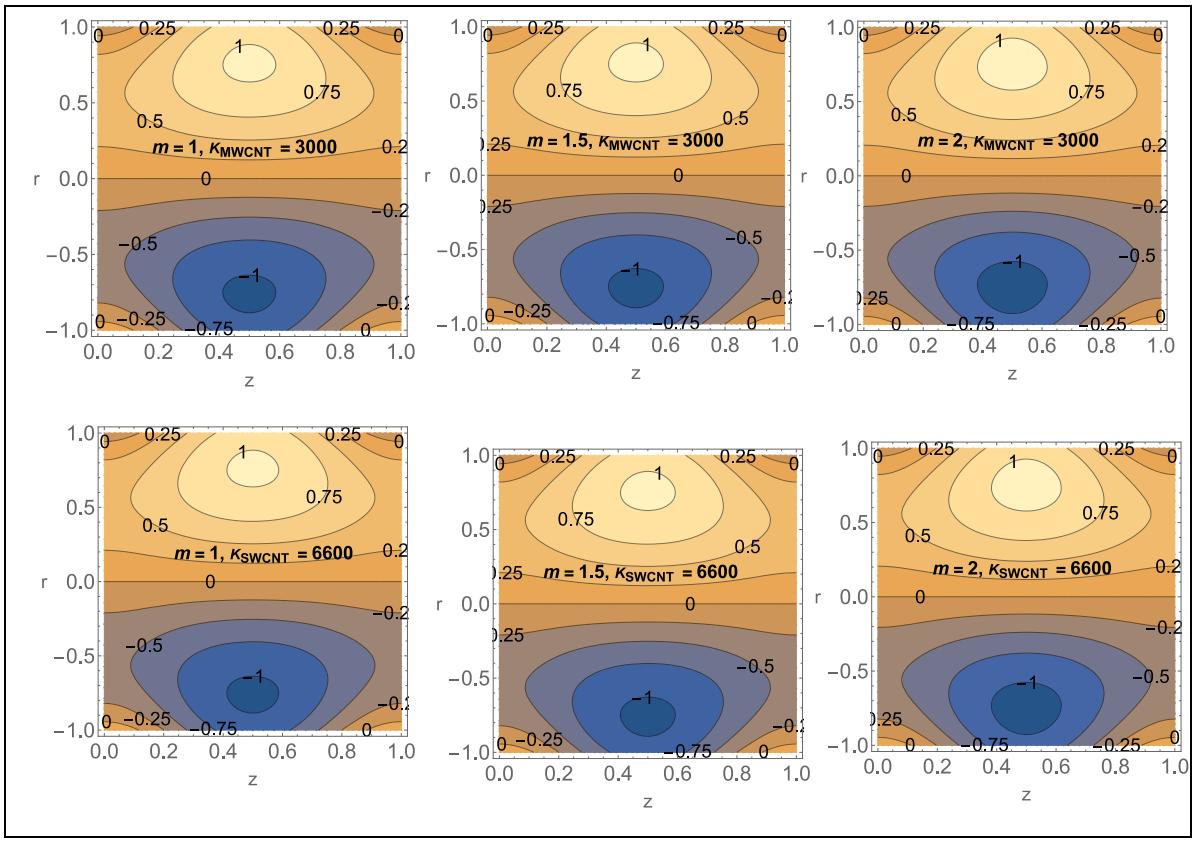

Figure 7: Streamlines with variation in electro-osmotic parameter (m) and thermal conductivity of MWCNT (K_{MWCNT}) and SWCNT (K_{SWCNT})

Figure 8 demonstrates that as the Helmholtz-Smoluchowski velocity (U_{Hs}) increases from negative values (opposing the electric field) to positive values (aided by the electric field), the size of the dual trapped boluses also increases. Additionally, the boluses are not fully formed and morph from the upper and lower walls, expanding into the core zone. Greater streamline intensities are computed for the SWCNT case (lower row) compared to the MWCNT case (upper row).

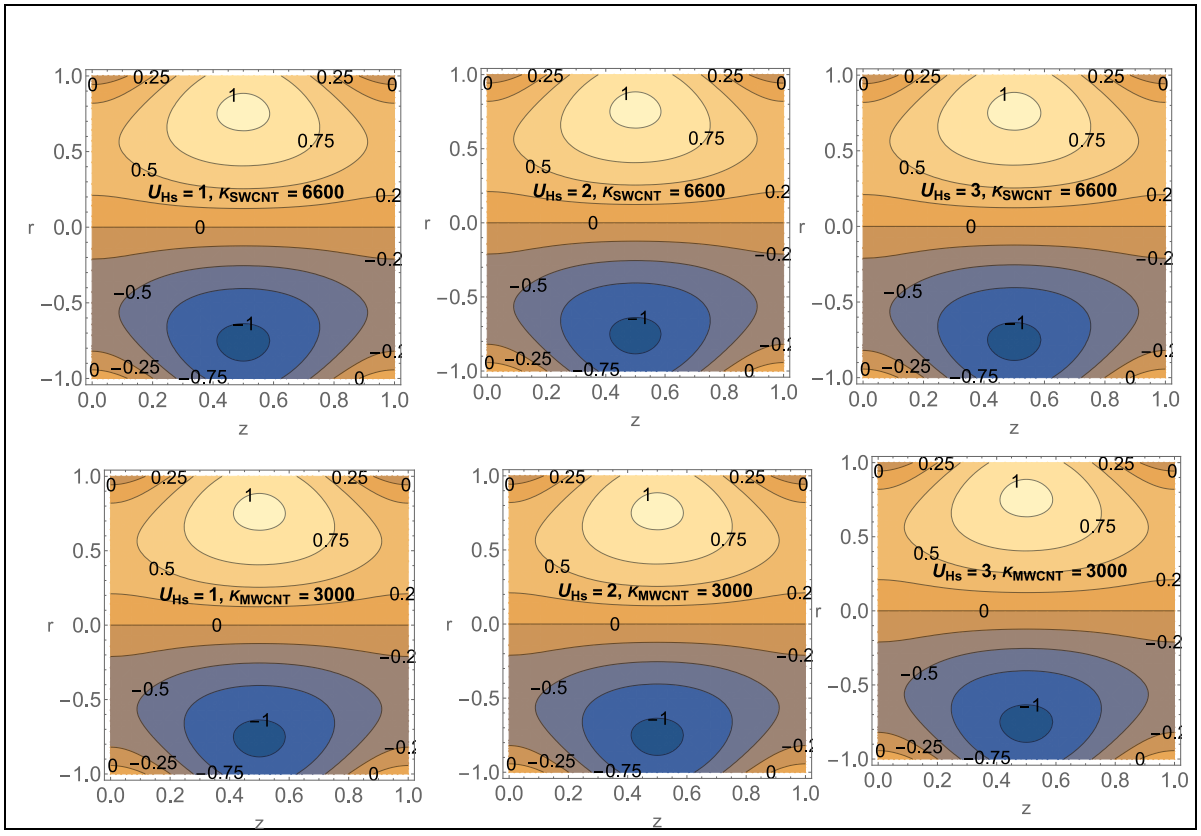

Figure 8: Streamlines computed with different Hemholtz-Smoluchowski velocity U_{Hs} and thermal conductivity of MWCNT (K_{MWCNT}) and SWCNT (K_{SWCNT})

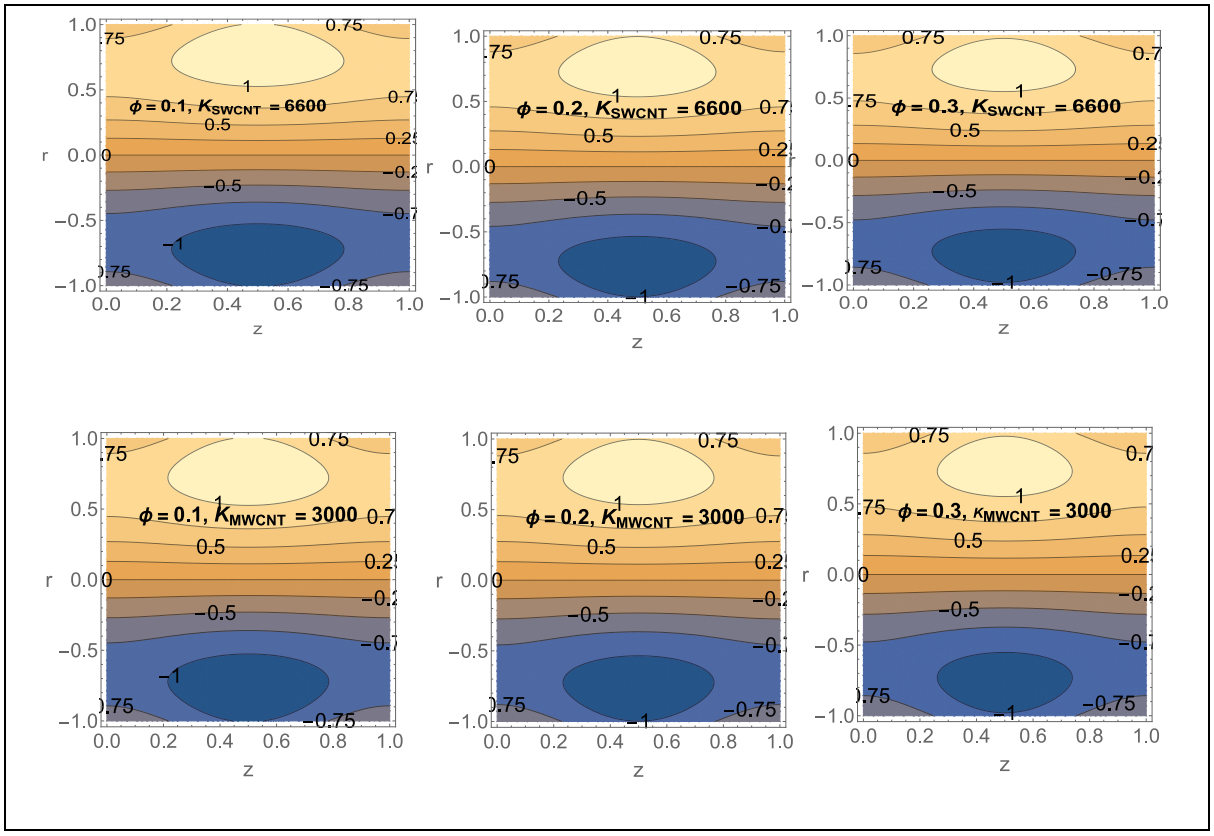

Figure 9 Streamline for carbon nanotube volume fraction (ϕ) and thermal conductivity of MWCNT (K_{MWCNT}) and SWCNT (K_{SWCNT}).

Figure 9. illustrates the thermal conductivity of multiwalled carbo nanotube $MWCNT$ (K_{MWCNT}) in the top row and single walled carbon nanotube $SWCNT$ (K_{SWCNT}) in the bottom row, alongside the streamlines for increasing carbon nanotube volume fraction (ϕ) values. As the carbon nanotube volume fraction (ϕ) Decreases, the size of the trapped zones, or boluses, at the top and bottom margins of the microtube also increases. Additionally, the partially produced twin upper and lower boluses significantly expand within the core zone. Although the structures of the trapped zones for $MWCNT$ (K_{MWCNT}) and $SWCNT$ (K_{SWCNT}) show relatively minor differences in calculations, the bolus shape extends noticeably as the carbon nanotube volume fraction (ϕ) increases from 0.3 to 0.8.

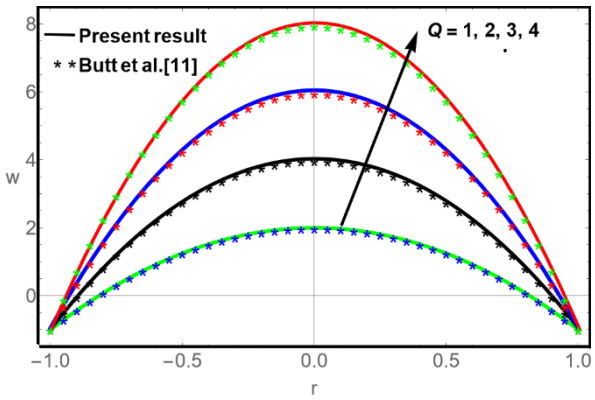

Figure 10. Comparison of present work with the work of Butt et al. [11], for different values of volume flow rate $\tilde{Q}$. When $m = 0, U_{Hs} = 0,\ \phi = 0$.

A comparison of the approximate solutions of present study with the existing standard results is portrays in Figure 10. It has been demonstrated to show the comparison of velocity profile w for the present study and the findings of Butt et al. [11], which is the particular case of present model for $m = 0, U_{Hs} = 0, Gr = 0, \phi = 0$ i.e. in the absence of electro-osmotic flow, Grashoff number and carbon nanotube volume fraction. From Figure 10, it can be concluded that the results of present model are closely align with the results of Butt et al. [11], for different values of volume flow rate $\tilde{Q}$, which is sufficient to say that the present model and results are validated.

Table 2. The comparison of velocity profile with existing literature Butt et al. [11] for different values of Q.

Butt et al. [11] at $M \approx 0$				Present work $m = 0, U_{Hs} = 0, Gr = 0, \phi = 0$			
$Q = 1$	$Q = 2$	$Q = 3$	$Q = 4$	$Q = 1$	$Q = 2$	$Q = 3$	$Q = 4$
-1	-1	-1	-1	-1	-1	-1	-1
1.24702	2.74503	4.24304	5.74105	1.250	2.750	4.250	5.75
1.98417	3.97361	5.96306	7.95251	2	4	6	8
1.24702	2.74503	4.24304	5.74105	1.250	2.750	2.750	2.750
-1	-1	-1	-1	-1	-1	-1	-1

5. CONCLUSIONS:

This study provides a comprehensive analysis of the electro-osmotic peristaltic streaming flow of fractional second grade viscoelastic nano fluids in permeable cylindrical tubes. The inclusion of single

and mixed carbon nanotubes presents new opportunities for optimizing fluid flow in various applications.

- Axial velocity is exhausted in the core section of the conduit with negative Helmholtz-Smoluchowski parameter (U_{Hs}) with reverse axial electrical field, whereas it is enhanced with positive Helmholtz-Smoluchowski parameter (aligned the axial electrical field). The opposite response is computed in the peripheral zones.
- The magnitude of axial velocity significantly enhances with enhancing the Darcy number Da, thermal source parameter (β_1), thermal Grashof number (Gr) and nanotube volume fraction (ϕ) in the central (core) region.
- Multiwalled carbon nano tube MWCNTs often attain higher temperatures than SWCNTs, and the temperature across the duct is greatly increased with the rising thermal source/sink parameter β_1. Conversely, the temperature is significantly reduced with an increasing carbon nanotube (CNT) volume fraction (ϕ)The amount of dual trapped boluses upsurges with the upsurge in the Helmholtz-Smoluchowski velocity, U_{hs} from negative (opposing electrical field) to positive values (assisted electrical field), although the number of boluses is not modified.
- When comparing the $SWCNT$ (K_{SWCNT}) example to the $MWCNT$ (K_{MWCNT}) case, a somewhat bigger bolus shape is seen.
- The axial pressure gradient continuously decreases with an increasing carbon nanotube (CNT) volume fraction $\phi$and increases with the electro-osmotic parameter (inverse Debye length, (m)the positive Helmholtz-Smoluchowski parameter ($U_{Hs)}$the Grashof number (Gr) and the thermal source parameter (β_1).
- The relationship between the pressure rise and the mean flow rate Q is inversely linear. The pressure rise is significantly increased by the electro-osmotic parameter m the positive Helmholtz-Smoluchowski parameter (U_{Hs}) and the thermal source parameter (β_1). Conversely, an increase in the viscoelastic material parameter (λ_1) results in a considerable suppression of the pressure rise.

The current study gives a solid platform for further studies to explore the bioheat transfer of electro-osmotically driven nanofluid pumping phenomena. Future research should focus on incorporating nonlinearities in electro-osmotic forces and fluid dynamics to more accurately represent the complex interactions within biological systems. Expanding the model to include multiphase fluid interactions would offer a deeper understanding of biofluid transport, particularly in scenarios where blood cells and plasma interact. Developing realistic geometrical models that reflect the irregular and varying cross-sections of biological tissues could enhance the real-world applicability of the findings. Additionally, exploring different boundary conditions representing various biological interfaces could provide a more nuanced understanding of the system's behaviour under different physiological conditions. Future work could also explore experimental validation and the impact of varying electric field strengths and CNT concentrations.

REFERENCES:

1. F. Yin and Y. Fung, *J. Fluid Mech.* 47, 93 **(1971).**
2. A.H. Shapiro, Jaffrin, and S.L. Weinberg, J. *Fluid Mechanics*. 37, 799 **(1969**).
3. J. Prakash, N. Balaji, E. P. Siva, M. Kothandapani, and A. Govindarajan, *Journal of Physics* 1000, 012166 **(2018).**
4. M. Kothandapani, J. Prakash, and V. Pushparaj, *Journal of Fluids* 2015, 561263 **(2015).**
5. M. Ajithkumar, P. Lakshminarayana, D. Tripathi, S. Kuharat and **O. Anwar Bég**, *Thermal Science and Engineering Progress*, **(2024).**
6. V.K. Narala and Dharmendra *Tripathi, Heat transfer* 1**(2020).**
7. N. B. Naduvinamani, Anita Siddayya Guttedar, and Laxmi Devindrappa, *Journal of Nanofluids*,11,737**(2022).**

8. C. Haseena, A. N. S. Srinivas, C. K. Selvi, S. Sreenadh, and B. Sumalatha, *Journal of Nanofluids*, 10,580 **(2021).**
9. M. M. Bhatti, A. Zeeshan, R. Ellahi, **O. Anwar Bég** and A. Kadir, *Chinese J. Physics.* 58, 222 **(2019).**
10. M. M. Channakote, D. V. Kalse, *Journal of Naval Architecture and Marine Engineering*, 19, 1**(2022).**
11. N.S. Akbar and A.W. Butt, *International Journal of Biomathematics*,6,150006 **(2014).**
12. S.U.S. Choi, *ASME FED. Proceedings of the ASME International Mechanical Engineering Congress and Exposition, San Francisco, USA* 66(1995).
13. J. Buongiorno, *ASME J. Heat Transfer*, 128, 240 **(2005).**
14. N. Biswas, Milan K. Mondal, Dipak Kumar Mandal, Nirmal K. Manna, Rama Subba Reddy Gorla, Ali J. Chamkha, *International Journal of Mechanical Sciences*,217, 107028 **(2022).**
15. N. Biswas, D. Chatterjee, S. Sarkar, N.K. and Manna, *International Journal of Numerical Methods for Heat & Fluid Flow*, 34,1021**(2024).**
16. D.K. Mandal, N. Biswas, N.K. Manna, et al. *The European Physical Journal Special Topics*. 231,2695**(2022).**
17. D.K. Mandal, N. Biswas, N.K. Manna, R.S.R. Gorla, and A.J. Chamkha, *International Journal of Numerical Methods for Heat & Fluid Flow*, 33,510 **(2023).**
18. A.S.Dogonchi, M. Waqas, S.R. Afshar. S.M. Seyyedi, M. Hashemi-Tilehnoee, Chamkha, A.J. and D.D. Ganji, *International Journal of Numerical Methods for Heat & Fluid Flow*, 30, 659 (2020).
19. P. Sreedevi, P. Sudarsana Reddy, Ali. J. Chamkha, *International Journal of Mechanical Sciences*, 135, 646 **(2018).**
20. N. S. Akbar, S. Nadeem, *Journal of Communications in Theoretical Physics.* 56 761**(2011).**
21. N.S. Akbar, *Journal of Computational and Theoretical Nanoscience*,11,1335 **(2014).**
22. Tripathi D and **Bég, O. Anwar**, *International Journal of Heat and Mass Transfer*, 70,61**(2014).**
23. S. Nadeem, Arshad Riaz R. Ellahi and N. S. Akbar, *Applied. Nanoscience.* 4,733 **(2014).**
24. N.S. Akbar, S. Nadeem, *Heat Transfer: Asian Research*, 41**, (2012).**
25. C. Haseena and A. N. S. Srinivas, *Journal of Nano fluid*, 6, 624 **(2017).**
26. D.Tripathi, S. Bhushan, **Bég, O. Anwar**. *et al. Journal of Hydrodynamics,* **30**, 1001 **(2018).**
27. B. Kumar a, G.S. Seth, R. Nandkeolyar, A. J. Chamkha**,** *International Journal of Thermal Sciences*.146,106101**(2019).**
28. N. Ali *et al*., *Nanomaterials (Basel)*. Jun; 11,1628 **(2021).**
29. Iqra Shahzadi, S. Nadeem, Faranak Rabiei, *Results in Physics*, 7, 667 **(2017).**
30. N. S. Akbar, Heat transfer and carbon nano tubes analysis for the peristaltic flow in a diverging tube. *Meccanica* 50, 39**(2015).**
31. T.Hayat, B.Ahmed, F.Abbasi, and B. Ahmad, *Computer Methods and Programs in Biomedicin*. 135, 141**(2016).**
32. S. Nadeem and Hina Sadaf, *J Braz. Soc. Mech. Sci. Eng*. 39, 117**(2017).**
33. M. Waqas, **O. Anwar Bég** and S. Kuharat *et al*, *International Journal of Hydrogen Energy*, (15 pages**) (2023).**
34. M. Kothandapani, and S. Srinivas, *Physics Letters A*, 4586 **(2008).**
35. V. P. Rathod and M.M. Channakote, *International Journal of Mathematical Archive*, 2, 1**(2012).**
36. N. S.Akbar, M. Raza, R. Ellahi, , *Computer Methods and Programs in Biomedicine*, 30, 22 **(2016).**
37. Zeeshan Asghar, Nasir Ali, Raheel Ahmed, Muhammad Waqas, Waqar Azeem Khan, *Computer Methods and Programs in Biomedicine*, 82, 105040 **(2019).**
38. S. Nadeem, Arshad Riaz R. Ellahi and N.S. Akbar, *Applied. Nanoscience.* 4:733(2014).
39. Channakote, Mahadev M. and Kalse, Dilipkumar V, *Applications and Applied Mathematics: An International Journal*, 16(2),1057 **(2021).**
40. K. Vajravelu, S. Sreenadh, R. Hemadri, K. Murugesan, *International Journal of Fluid Mechanics Research*. 36, 244 **(2009).**

41. K.Vajravelu S. Sreenadh K.Rajanikanth, and Lee Changhoon, *Real World Applications*, 13, 6 (2012).
42. S. Chakraborty, *Journal of Physics D Applied Physics*, 39, 535, **(2006).**
43. D. Tripathi, A. Yadav and **O. Anwar Bég**, *European Physical Journal Plus (Italy) 132, 173* **(2017).**
44. N. Ali, S. Hussain, K. Ullah, **O. Anwar Bég**, *European Physical Journal Plus*, 134, 1**(2019).**
45. A.A.Abbasi, F.Mabood, W. Farooq, and S. Khan,. *International Journal of Communication in Heat and Mass Transfer*. **123**, 105183 (2021).
46. S. Waheed, S. Noreen, Hussanan, *Applied Sciences*.9, 2164 **(2019).**
47. Mahadev Madivalappa Channakote, Dilipkumar Vilasrao Kalse, Asha Shivappa Kotnurkar, & Shekar Marudappa. *Journal of Advanced Research in Fluid Mechanics and Thermal Sciences*, 114,50**(2024).**
48. M.M. Channakote, S.K Asha, Heat transfer and electro-osmotic analysis on peristaltic pumping of a fractional second-grade fluid through a cylindrical tube, *International Journal of Computational Materials Science*, **12**, 2350007 **(2023).**
49. V.P.Rathod, and M.Mahadev, *Therm. Sci*. **18** 1109-1118 (2014).
50. A.M.Abd-Alla, S.M.Abo-Dahab, T.Esraa, M. A. Abdelhafez, *Scintific Reports*, 12, 10608 **(2022).**
51. D.Tripathi and **O. Anwar Bég**, *Computer Methods in Biomechanics and Biomedical Engineering*, 18, 1 **(2014).**
52. D. Tripathi., *Thermal. Science*. **15**, S167-S173 **(2011).**
53. Guo, Xiaoyi, and Haitao Qi. *Micromachines* 8, 341**(2017).**
54. M. Hameed, , A.A. Khan, R.Ellahi, M. Raza, *Engineering Science and Technology-An International Journal*.**18,** 496.(2015).